

# Multiple scattering of ultrasound in weakly inhomogeneous media: Application to human soft tissues

Alexandre Aubry<sup>a)</sup> and Arnaud Derode

*Institut Langevin, ESPCI ParisTech, CNRS UMR 7587, Université Denis Diderot (Paris VII), 10 rue Vauquelin, 75005 Paris, France*

(Received 5 May 2010; revised 23 September 2010; accepted 1 October 2010)

Waves scattered by a weakly inhomogeneous random medium contain a predominant single-scattering contribution as well as a multiple-scattering contribution which is usually neglected, especially for imaging purposes. A method based on random matrix theory is proposed to separate the single- and multiple-scattering contributions. The experimental setup uses an array of sources/receivers placed in front of the medium. The impulse responses between every couple of transducers are measured and form a matrix. Single-scattering contributions are shown to exhibit a deterministic coherence along the antidiagonals of the array response matrix, whatever the distribution of inhomogeneities. This property is taken advantage of to discriminate single- from multiple-scattered waves. This allows one to evaluate the absorption losses and the scattering losses separately, by comparing the multiple-scattering intensity with a radiative transfer model. Moreover, the relative contribution of multiple scattering in the backscattered wave can be estimated, which serves as a validity test for the Born approximation. Experimental results are presented with ultrasonic waves in the megahertz range, on a synthetic sample (agar-gelatine gel) as well as on breast tissues. Interestingly, the multiple-scattering contribution is found to be far from negligible in the breast around 4.3 MHz. © 2011 Acoustical Society of America. [DOI: 10.1121/1.3506343]

PACS number(s): 43.60.Gk, 43.20.Fn, 43.80.Ev, 43.35.Bf [RKS]

Pages: 225–233

## I. INTRODUCTION

Standard imaging techniques such as ultrasonic echography,<sup>1</sup> radar,<sup>2</sup> or optical coherence tomography<sup>3</sup> are based on the same principle. One or several source(s) emit(s) a wave into the medium to be imaged. It is reflected by the inhomogeneities of the medium, and the backscattered wave is measured by the same or other sensor(s). It contains two contributions:

- (1) A single-scattering contribution (path  $s$  in Fig. 1): The incident wave undergoes only one scattering event before coming back to the sensor(s). This is the contribution which is used in imaging because there is a direct relation between the arrival time  $t$  of the echo and the distance  $d$  between the sensors and the scatterer,  $t = 2d/c$  ( $c$  is the sound velocity). An image of the medium reflectivity can be built from measured signals.
- (2) A multiple-scattering contribution (path  $m$  in Fig. 1): The wave undergoes several scattering events before reaching the sensor. Multiple scattering occurs when scatterers are strongly diffusive and/or highly concentrated. There is no correspondence between the arrival time  $t$  and the position of a scatterer. Thus, classical imaging fails in multiple-scattering media.<sup>4–7</sup>

Standard imaging techniques rely on the single-scattering assumption (first Born approximation). However, there is no such thing as a purely single-scattering medium. A multiple-scattering contribution always exists, albeit negligible compared to single scattering. Naturally for imaging purposes, one tries to reduce the influence of multiple scattering, for

instance, by choosing an appropriate frequency domain where multiple scattering is not too strong.<sup>8</sup> Focused beamforming with an array of transducers, or more generally synthetic aperture techniques,<sup>2</sup> are also a way to enhance the single-scattering contribution. It should be noted that even though multiple scattering is considered as the enemy of classical imaging techniques, studying it may bring additional information about the scattering structure. Indeed, a wave undergoing multiple scattering can be thought of as a random walker,<sup>9</sup> with two essential parameters: The elastic mean-free path  $l_e$  and the diffusion constant  $D$ . Measuring these parameters is a way to characterize the microarchitecture of the scattering medium.<sup>10,11</sup> Yet in weakly inhomogeneous media where the first Born approximation is reasonably valid (especially human soft tissues probed by ultrasound in the megahertz range), it is a challenge to study multiple-scattering parameters because of the predominance of single scattering.

Recently, an original technique has been proposed to separate the single-scattered echo of a target drowned in a predominant multiple-scattering background.<sup>8,12</sup> The method was based on a matrix approach. It has been successfully applied to target detection and imaging in highly scattering media. In this paper, we are also interested in discriminating single-scattering and multiple-scattering contributions from the total response of an unknown medium, based on matrix properties. However, the present approach is different from earlier works,<sup>8,12</sup> both in terms of method and applications. The situation we consider here is exactly the opposite: We want to extract the multiple-scattering contribution from predominantly single-scattered waves in a weakly scattering media. Moreover, the method is based on a singular value decomposition (SVD) applied to the antidiagonals of the array response matrix and not to the array response matrix

<sup>a)</sup>Author to whom correspondence should be addressed. Electronic mail: alexandre.aubry@espci.fr

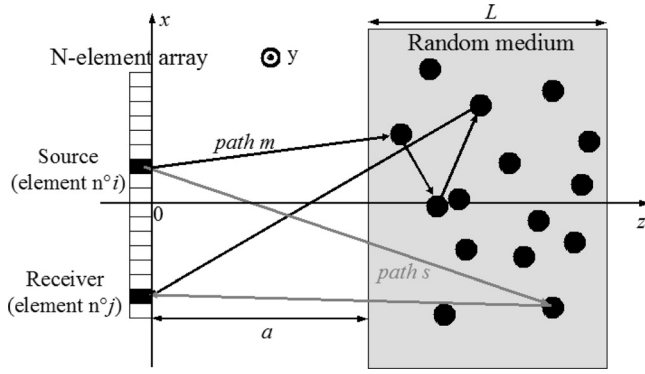


FIG. 1. Experimental setup: A 125-element linear array is placed in front of a random medium at a distance  $a$ . The whole setup is immersed in a water tank.

itself. The distinction between single- and multiple-scattering subspaces is then performed using random matrix theory (RMT),<sup>13,14</sup> as it will be detailed in the Sec. IV.

The interest of this work is twofold. First, once single- and multiple-scattering contributions are isolated, the proportion of multiple scattering within the wave response of the medium can be evaluated. This figure can be used as an indicator for the validity of the single-scattering (Born) approximation, which is the basis of classical imaging techniques. Note, however, that the purpose of this study is not to improve imaging of weakly scattering media. The second interest of this work is to provide a new tool for the characterization of weakly scattering media. More precisely, we will show how the multiple-scattering contribution, once it is isolated, can be taken advantage of in order to estimate the scattering mean-free path  $l_e$  independently from the absorption mean-free path  $l_a$ , thus discriminating absorption and scattering losses.

The experimental results we present were obtained with pulsed ultrasonic waves first in a synthetic medium (agar-gelatine gel) around 3 MHz and then in breast tissues around 4.3 MHz, but the principle of the technique can be applied to all fields of wave physics (e.g., seismology, electromagnetism, acoustics, etc.) for which the multi-element array technology is available and provides time-resolved measurements of the amplitude and the phase of the wave-field.

## II. TRANSDUCERS' ARRAY CONFIGURATION

We use an  $N$ -element ultrasonic array (here,  $N = 125$ ). The array is placed at a distance  $a$  from the random scattering sample under investigation (see Fig. 1). The first step of the experiment consists in measuring the inter-element matrix. A sinusoidal burst of length  $\delta t$  at the central frequency  $f_c$  is emitted from transducer  $i$  into the scattering medium. Typical values here are  $\delta t \sim 1 \mu s$  and  $f_c \sim 3$  MHz. The back-scattered wave is recorded with the  $N$  transducers of the same array, which yields a set of impulse responses  $h_{ij}(t)$  ( $j = 1, \dots, N$  denotes the receiver index). The operation is repeated for the  $N$  emitting transducers. The responses  $h_{ij}(t)$  form the  $N \times N$  impulse response matrix  $\mathbf{H}(t)$ . Because of reciprocity,  $h_{ij}(t) = h_{ji}(t)$  and  $\mathbf{H}(t)$  is symmetric. A short-time Fourier analysis of the impulse response matrix  $\mathbf{H}$  is performed. The time signals  $h_{ij}(t)$  are truncated into  $\Delta t$ -long

overlapping windows:  $k_{ij}(T, t) = h_{ij}(T - t)W_R(t)$  with  $W_R(t) = 1$  for  $t \in [-\Delta t/2, \Delta t/2]$ ,  $W_R(t) = 0$  anywhere else. The value of  $\Delta t$  is chosen so that signals associated with the same scattering event(s) within the medium arrive in the same time window.<sup>15</sup> Typical values here are  $\Delta t \sim 10 \mu s$ . A Fourier analysis of  $\mathbf{K}(T, t)$  is achieved by means of a discrete Fourier transform. A response matrix  $\mathbf{K}(T, f)$  is finally obtained at each time  $T$  and frequency  $f$ . The single- and multiple-scattering contributions can now be discriminated with the help of a matrix manipulation.

## III. THE SIGNATURE OF SINGLE SCATTERING

When studying the array response matrices  $\mathbf{K}(T, f)$ , the predominance of single scattering manifests itself by the presence of a long-range deterministic coherence along the anti-diagonals of the matrix, whatever the distribution of scatterers.<sup>8,12,15</sup> As an example, Fig. 2 shows the real part of one of the matrices,  $\mathbf{K}$ , in the case of a synthetic medium (agar-gelatine gel) which is enough weakly scattering for the Born approximation to be valid. Even if the inhomogeneities are randomly distributed,  $\mathbf{K}$  obviously exhibits some kind of coherence along its anti-diagonals (i.e., for matrix elements  $k_{ij}$  such that  $i + j = \text{constant}$ ). This coherence is a typical signature of single scattering, and it vanishes when multiple scattering dominates. This has been thoroughly explained in Refs. 15, 12, and 15, and we briefly recall the main argument here.

Generally, the  $k_{ij}(T, f)$  can be written as the sum of single- and multiple-scattering contributions:

$$k_{ij}(T, f) = k_{ij}^S(T, f) + k_{ij}^M(T, f). \quad (1)$$

Under the paraxial approximation, the distance between the origin  $(0, 0)$  and an observer  $(x, R)$  located slightly off-axis ( $x \ll R$ ) is  $\sqrt{R^2 + x^2} = R + x^2/(2R)$ . As a result, the phase shift undergone by a wave traveling from a source with coordinates  $(0, x_i)$ , scattered by a point  $(X_d, R)$ , and received in the plane of the source at  $(0, x_j)$  reads

$$\exp[2jkr] \exp\left[jk \frac{(x_i - X_d)^2}{2R}\right] \exp\left[jk \frac{(x_j - X_d)^2}{2R}\right],$$

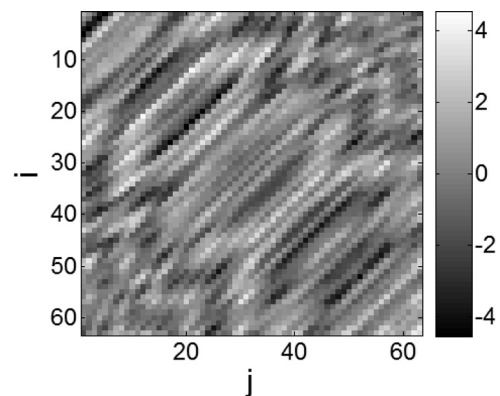


FIG. 2. Real part of matrix  $\mathbf{K}$  obtained in a gel (5% gelatine, 3% agar-agar) at time  $T = 114 \mu s$  and frequency  $f = 3.05$  MHz. The source-sample distance was  $a = 50$  mm.

with  $k$  as the wavenumber. The quadratic phase terms can be factorized since

$$(x_i - X_d)^2 + (x_j - X_d)^2 = \frac{(x_i - x_j)^2}{2} + \frac{(x_i + x_j - 2X_d)^2}{2}. \quad (2)$$

Consider an ensemble of scatterers randomly distributed. As long as only the first and the last scattering of every scattering path are identical (which is naturally the case, if only single scattering takes place), the coefficients of the array response matrix at time  $T$  and frequency  $f$  will be proportional to

$$k_{ij}^S(T, f) \propto \exp(j2kR) \sum_{d=1}^{N_d} A_d \exp \left[ jk \frac{(x_i - X_d)^2}{2R} \right] \times \exp \left[ jk \frac{(x_j - X_d)^2}{2R} \right], \quad (3)$$

with  $R = cT/2$  and  $N_d$  the number of scatterers contained in the isochronous volume.  $A_d$  depends on the reflectivity of the scatterer.  $A_d$  and  $X_d$  are random variables, so  $k_{ij}^S$  is itself random. Interestingly, applying the factorization of Eq. (2) to Eq. (3), a deterministic relation arises along the antidiagonals of  $\mathbf{K}^S$ :

$$\beta_m = \frac{k_{i-m, i+m}(T, f)}{k_{ii}(T, f)} = \exp \left[ jk \frac{(m\delta x)^2}{R} \right], \quad (4)$$

with  $\delta x$  denoting the array pitch and  $2m\delta x$  the distance between two array elements ( $i - m$  and  $i + m$ ) on the same antidiagonal. Equation (4) implies that as long as there is only single scattering, there must be a form of coherence, a long-range deterministic relation, between the elements of the array response matrix, whatever the realization of disorder. On the contrary, when multiple scattering occurs (except for recurrent scattering paths,<sup>16</sup> but this contribution is negligible in weakly scattering media), the elements  $k_{ij}^M$  cannot be factorized, and there is no such long-range deterministic coherence.<sup>8,12,15</sup>

#### IV. SEPARATION OF SINGLE AND MULTIPLE SCATTERING

The key to separate single- ( $\mathbf{K}^S$ ) and multiple- ( $\mathbf{K}^M$ ) scattering contributions is the particular coherence of  $\mathbf{K}^S$  along its antidiagonals. In previous works,<sup>8,12</sup>  $\mathbf{K}^S$  was extracted from  $\mathbf{K}$  by projecting the antidiagonals of  $\mathbf{K}$  along the vector  $[\beta_m]$  of Eq. (4). But the simple form taken by Eq. (4) results from a series of assumptions (paraxial approximation, point-like array elements, and scatterers) all of which do not apply to our experimental configuration. In order to separate  $\mathbf{K}^S$  and  $\mathbf{K}^M$ , the method proposed in this paper is much less restrictive. We do not assume that Eq. (4) exactly applies; we only assume that because of single scattering there must be a deterministic coherence between the antidiagonal elements of  $\mathbf{K}^S$ , but we do not suppose we know its exact form.

Under these conditions, the separation between  $\mathbf{K}^S$  and  $\mathbf{K}^M$  will essentially rely on a SVD of the antidiagonals of  $\mathbf{K}$ . This separation is a three-step process:

- (1) Rotation of each matrix  $\mathbf{K}$  and construction of two submatrices  $\mathbf{A}_1$  and  $\mathbf{A}_2$ .
- (2) Filtering of matrices  $\mathbf{A}_r$  ( $r = 1, 2$ ):  $\mathbf{A}_r$  is decomposed as the sum of two matrices:  $\mathbf{A}_r = \mathbf{A}_r^S + \mathbf{A}_r^M$ , where  $\mathbf{A}_r^S$  and  $\mathbf{A}_r^M$  contain the single- and multiple-scattering signals, respectively.
- (3) Construction from  $\mathbf{A}_r^S$  and  $\mathbf{A}_r^M$  of the single- and multiple-scattering matrices  $\mathbf{K}^S$  and  $\mathbf{K}^M$ .

The first and third steps (rotation of data) have already been presented in previous works<sup>8,12</sup> and will be briefly recalled in Secs. IV A and IV C. On the contrary, the second step (SVD of antidiagonals) constitutes the core of the method and differs completely from the previous approach.<sup>8,12</sup> The corresponding matrix operations are explained in detail in Sec. IV B.

##### A. First step

A rotation of matrix data is achieved as depicted in Fig. 3. It consists in building two matrices  $\mathbf{A}_1$  and  $\mathbf{A}_2$  from matrix  $\mathbf{K} = [k_{ij}]$ :

$$\mathbf{A}_1 = [a_{1uv}] \text{ of dimension } (2M - 1) \times (2M - 1), \text{ such that } a_{1[u, v]} = k[u + v - 1, v - u + 2M - 1], \quad (5)$$

$$\mathbf{A}_2 = [a_{2uv}] \text{ of dimension } (2M - 2) \times (2M - 2), \text{ such that } a_{2[u, v]} = k[u + v, v - u + 2M - 1], \quad (6)$$

where  $M = (N + 3)/4$ . Here,  $N = 125$  and so  $M = 32$  is an even number. The columns of matrices  $\mathbf{A}_1$  and  $\mathbf{A}_2$  correspond to the antidiagonals of  $\mathbf{K}$  (see Fig. 3). In Sec. IV B, we will no longer make the difference between matrices  $\mathbf{A}_1$  and  $\mathbf{A}_2$  because they are filtered in the same way. They will be called  $\mathbf{A}$  indifferently.  $L$  is the dimension of  $\mathbf{A}$ . For matrix  $\mathbf{A}_1$ ,

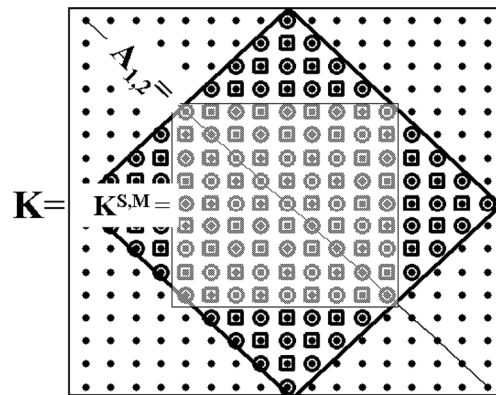


FIG. 3. Example of a matrix  $\mathbf{K}$  of dimension  $N = 17$ . The black points represent the elements  $k_{ij}$  of  $\mathbf{K}$ . The antidiagonals of  $\mathbf{K}$  are the columns of matrices  $\mathbf{A}_1$  and  $\mathbf{A}_2$ . Circles and squares represent the elements of  $\mathbf{A}_1$  and  $\mathbf{A}_2$ , respectively. Once single- and multiple-scattering contributions are separated, the final matrices  $\mathbf{K}^S$  and  $\mathbf{K}^M$  have  $(2M - 1) \times (2M - 1)$  elements (central square).

$L = 2M - 1$ ; for matrix  $\mathbf{A}_2$ ,  $L = 2M - 2$ . Because of spatial reciprocity,  $\mathbf{K}$  is symmetric ( $k_{ij} = k_{ji}$ ). Thus,  $\mathbf{A}$  exhibits also a symmetry: Each line of its upper part is identical to a line of its lower part. The symmetry axis is shown as a black line in Fig. 3 and corresponds to the diagonal of the matrix  $\mathbf{K}$ . So, each column of the matrix  $\mathbf{A}$  contains only  $M$  independent coefficients, even if its dimension  $L$  is larger than  $M$ .

## B. Second step

$\mathbf{A}$  can be written as a sum of two matrices  $\mathbf{A}^S$  and  $\mathbf{A}^M$ , which correspond, respectively, to the single- and multiple-scattering contributions,

$$\mathbf{A} = \mathbf{A}^S + \mathbf{A}^M. \quad (7)$$

Contrary to previous works,<sup>8,12</sup> the technique we propose in this paper consists in separating single and multiple scattering by achieving the SVD of the matrix  $\mathbf{A}$ . The SVD decomposes a matrix into two subspaces: A *signal* subspace (a matrix characterized by an important correlation between its lines and/or columns) and a *noise* subspace (a random matrix without any correlations between its entries). When the SVD is applied to the matrix  $\mathbf{A}$ , the *signal* subspace (i.e., the largest singular values) corresponds to  $\mathbf{A}^S$  (the single-scattering contribution characterized by a long-range correlation along its columns) and the *noise* subspace (i.e., the smallest singular values) corresponds to  $\mathbf{A}^M$  (the multiple-scattering contribution).

The SVD of matrix  $\mathbf{A}$  is given by

$$\mathbf{A} = \mathbf{U}\mathbf{\Lambda}\mathbf{V}^\dagger = \sum_{k=1}^L \lambda_k \mathbf{U}_k \mathbf{V}_k^\dagger, \quad (8)$$

where  $\mathbf{U}$  and  $\mathbf{V}$  are square unitary matrices of dimension  $L$ . Their respective columns  $\mathbf{U}_k$  and  $\mathbf{V}_k$  correspond to the singular vectors associated to the singular value  $\lambda_k$ .  $\mathbf{\Lambda}$  is a square diagonal matrix of dimension  $L$ , containing the real positive singular values  $\lambda_k$  in decreasing order ( $\lambda_1 > \lambda_2 > \dots > \lambda_L$ ). Actually,  $\mathbf{A}$  has only  $M$  non-zero singular values since it contains only  $M$  independent lines, and hence Eq. (8) becomes

$$\mathbf{A} = \mathbf{U}\mathbf{\Lambda}\mathbf{V}^\dagger = \sum_{k=1}^M \lambda_k \mathbf{U}_k \mathbf{V}_k^\dagger. \quad (9)$$

The issue is to determine which rank of singular value separates the *signal* subspace (single scattering) from the *noise* subspace (multiple scattering). If Eq. (4) were strictly true, the single-scattering contribution  $\mathbf{A}^S$  would be of rank 1 and only the first singular space associated to the first singular value  $\lambda_1$  would correspond to the signal subspace. But when assumptions leading to Eq. (4) do not strictly hold,  $\mathbf{A}^S$  is no longer of rank 1, and several singular spaces (associated to the largest singular values) are needed to fully describe the signal subspace. This happens for instance when scatterers are not pointlike or when the paraxial approximation does not hold. We have to define a threshold to discriminate the signal and noise subspaces, with the help of RMT.<sup>13,14</sup>

By convention and for the sake of simplicity, the singular values  $\lambda_k$  are first normalized by their quadratic mean,

$$\tilde{\lambda}_k = \frac{\lambda_k}{\sqrt{M^{-1} \sum_{q=1}^M \lambda_q^2}}. \quad (10)$$

For a random matrix of dimension  $P \times Q$  (with  $1 \ll P < Q$ ), whose entries are complex random variables, independently and identically distributed, the probability density function  $\rho(\lambda)$  of the normalized singular values  $\tilde{\lambda}_k$  is given by:<sup>14</sup>

$$\rho(\lambda) = \frac{1}{\pi\lambda} \sqrt{(\lambda_{\max}^2 - \lambda^2)(\lambda^2 - \lambda_{\min}^2)} \quad (11)$$

for  $\lambda_{\min} < \lambda < \lambda_{\max}$  and 0 otherwise, with

$$\lambda_{\max,\min} = 1 \pm \sqrt{P/Q}. \quad (12)$$

For random matrices of large dimensions, the singular value spectrum has bounded support. In our case,  $\mathbf{A}$  is a square matrix of dimension  $L \times L$ . Yet, as it contains only  $M$  independent lines, it is equivalent to a rectangular  $M \times L$  matrix. If it were truly random (which is expected to be the case of the multiple-scattering contribution), its largest singular value should not exceed  $\lambda_{\max} = 1.71$ . This value is obtained from Eq. (12), with  $P = M = 32$  and  $Q = L = 63$ .

It should be noted that rigorously  $L$  and  $M$  are not large enough for the asymptotic law [Eq. (11)] to apply. Actually the first singular value  $\tilde{\lambda}_1$  obeys a complicated law, known as the Tracy–Widom distribution,<sup>17</sup> which is of unbounded support. The probability for  $\tilde{\lambda}_1$  to be larger than  $\lambda_{\max}$  can be computed: It is found to be  $\sim 0.08$  for  $P = M = 32$  and  $Q = L = 63$ . The presence of correlations between matrix entries also induces a deviation from Eq. (11), as we will see later. For the sake of simplicity, we admit for now that within an acceptable probability of error, the singular values are upper bounded by  $\lambda_{\max}$ .

According to Eq. (7),  $\mathbf{A}$  is the sum of a matrix  $\mathbf{A}^S$  of rank  $p < M$  (associated to single scattering) and a matrix  $\mathbf{A}^M$  of rank  $M$  (associated to multiple scattering). Sengupta and Mitra<sup>14</sup> have shown that the  $(M - p)$  smallest singular values (linked to the noise subspace) exhibit the same distribution as singular values of a random matrix whose size is  $(M - p) \times L$ . Let  $\lambda_{\max}^{(q)}$  denote the upper bound of the singular values distribution in the case of a random matrix of dimension  $(M - q) \times L$ , we have

$$\lambda_{\max}^{(q)} = 1 + \sqrt{(M - q)/L}. \quad (13)$$

From this property, one can propose a way to separate the signal and noise subspaces of  $\mathbf{A}$ . We first consider the first singular value  $\tilde{\lambda}_1$  upon normalization [Eq. (10)]. If  $\tilde{\lambda}_1$  is larger than  $\lambda_{\max}^{(0)}$  [Eq. (13)], it means that the first singular space  $\lambda_1 \mathbf{U}_1 \mathbf{V}_1^\dagger$  is associated with the signal subspace. Then, we iterate the process and consider the second singular value;  $\lambda_k$  is once again renormalized, considering only the singular values from  $k = 2$ :

$$\tilde{\lambda}_2 = \frac{\lambda_2}{\sqrt{(M - 1)^{-1} \sum_{k=2}^M \lambda_k^2}}. \quad (14)$$

The threshold value  $\lambda_{\max}$  to consider this time is the one obtained for a random matrix of size  $(M - 1) \times L$ , i.e.,  $\lambda_{\max}^{(1)}$  [Eq. (13)]. If  $\tilde{\lambda}_2 > \lambda_{\max}^{(1)}$ , the second singular space  $\lambda_2 \mathbf{U}_2 \mathbf{V}_2^\dagger$  is also linked to the single-scattering contribution, and we iterate the process once more until rank  $p + 1$ , for which  $\tilde{\lambda}_{p+1} < \lambda_{\max}^{(p)}$ . Finally, we obtain a threshold rank  $p$  which allows to separate the signal ( $\mathbf{S}$ ) and noise ( $\mathbf{N}$ ) subspaces,

$$\mathbf{S} = \sum_{k=1}^p \lambda_k \mathbf{U}_k \mathbf{V}_k^\dagger, \quad \mathbf{N} = \sum_{k=p+1}^M \lambda_k \mathbf{U}_k \mathbf{V}_k^\dagger. \quad (15)$$

Ideally,  $\mathbf{S}$  should be devoid of multiple scattering. This is not strictly true because multiple-scattering signals are not strictly orthogonal to the single-scattering subspace. Let  $\sigma_S^2$  and  $\sigma_M^2$  be the power of single- and multiple-scattering signals, respectively. The typical amplitude of the remaining multiple-scattering contribution in  $\mathbf{S}$  is  $\sigma_M \sqrt{p/2M} (\ll \sigma_S)$ .<sup>18</sup> If we neglect this residual term, we have separated single- and multiple-scattering contributions:  $\mathbf{A}^S \simeq \mathbf{S}$  and  $\mathbf{A}^M \simeq \mathbf{N}$ . The whole separation process is summarized in Fig. 4.

Note that a multiple-scattering rate  $\gamma$  can be directly measured from the singular values,  $\lambda_k$ , of  $\mathbf{A}$ . The sum of the square of all the singular values corresponds to the total intensity backscattered by the medium toward the transducers' array. Hence, a multiple-scattering rate  $\gamma$  can be estimated from the singular values,  $\lambda_k$ , of  $\mathbf{A}$ :

$$\gamma = \frac{\sum_{k=p+1}^M \lambda_k^2}{\sum_{k=1}^M \lambda_k^2}. \quad (16)$$

Until now, for simplicity we have implicitly assumed that along the antidiagonals of  $\mathbf{K}^M$  (or the columns of  $\mathbf{A}^M$ )

the matrix elements are completely decorrelated. However, experimentally short-range correlations may exist between elements, mostly because of mechanical coupling between neighboring transducers and of the coherence length of the diffuse wave-field.<sup>12,15</sup> Correlations between matrix elements can be taken into account theoretically.<sup>14</sup> Consequently, the actual probability density function  $\rho(\lambda)$  is more complicated than the simple result of Eq. (11), which modifies the upper bound  $\lambda_{\max}^{(q)}$ .<sup>12,15</sup> In practice,  $\lambda_{\max}^{(q)}$  has to be computed numerically, based on an acceptable probability of error (typically 1%).<sup>18</sup>

This technique of separation is based on the fact that the first singular value exceeds the value  $\lambda_{\max}$ , otherwise there is no separation between single and multiple scattering, and the whole signal is considered to be associated with multiple scattering. So, this approach is not well suited for strongly diffusive media, i.e., random media for which the multiple-scattering contribution is predominant.<sup>8,12</sup>

### C. Third step

The third step is the reverse of the first one. From  $\mathbf{A}^S$  and  $\mathbf{A}^M$ , two matrices  $\mathbf{K}^S$  and  $\mathbf{K}^M$ , of dimension  $(2M - 1) \times (2M - 1)$ , are built (see Fig. 3) with a change of coordinates, back to the original system:

- (1) if  $(i - j)/2$  is an integer, then  $k^{S,M}[i, j] = a_1^{S,M}[(i - j)/2 + M, (i + j)/2]$
- (2) if  $(i - j)/2$  is not an integer, then  $k^{S,M}[i, j] = a_2^{S,M}[(i - j - 1)/2 + M, (i + j - 1)/2]$ .

$\mathbf{K}^S$  contains the single-scattering contribution (plus a residual multiple-scattering contribution) and  $\mathbf{K}^M$  contains the multiple-scattering contribution.

## V. CHARACTERIZATION OF A WEAKLY SCATTERING MEDIUM

The experimental setup has already been described in Sec. II and is shown in Fig. 1. The experiment takes place in a water tank. The ultrasonic array has  $N = 125$  elements. The emitted signal is a sinusoidal burst of length  $\delta t = 2.5 \mu\text{s}$  at the central frequency (3 MHz). The sampling frequency is 20 MHz. Each array element is 0.39 mm in size, and the array pitch  $\delta x$  is 0.417 mm. The source-sample distance is  $a = 50$  mm. The first random medium of interest is a gel composed of 5% of gelatine and 3% of agar. In this kind of medium and frequency range, the single-scattering contribution is by far predominant.<sup>19</sup> The thickness  $L$  of the scattering slab is 100 mm. Once the inter-element matrix  $\mathbf{H}$  is measured, the short-time Fourier analysis described in Sec. II yields a set of response matrices  $\mathbf{K}(T, f)$ . Then, the separation of single and multiple scattering is achieved as described in Sec. IV.

Figure 5 shows a typical experimental result, taken at time  $T = 114 \mu\text{s}$  and frequency  $f = 3.05$  MHz. Note that the separation rank between the signal and noise subspaces is here  $p = 2$ , which confirms that Eq. (4) does not strictly hold.  $\mathbf{K}^S$  exhibits the deterministic coherence along the antidiagonals [Fig. 5(a)], which is characteristic of single scattering. Obviously,  $\mathbf{K}^S$  is very close to the raw matrix  $\mathbf{K}$  (Fig. 2),

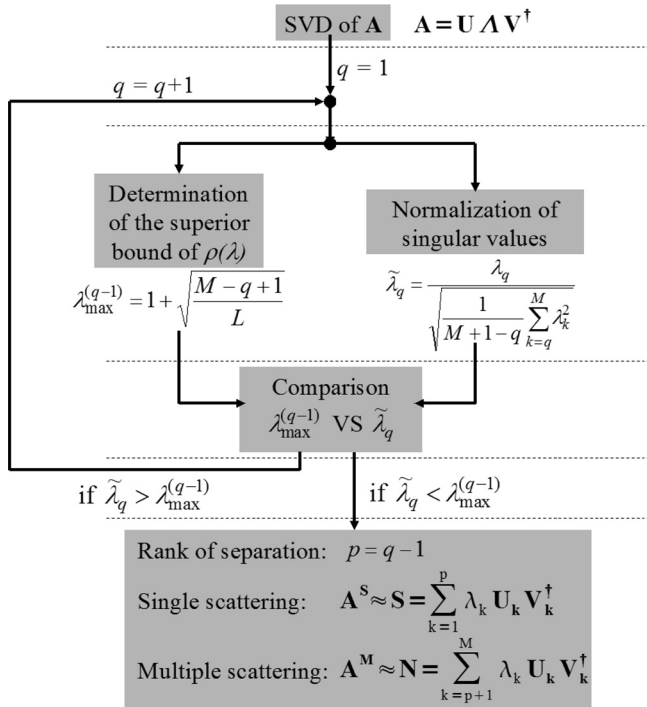


FIG. 4. Principle of the separation between the single- and multiple-scattering contributions.

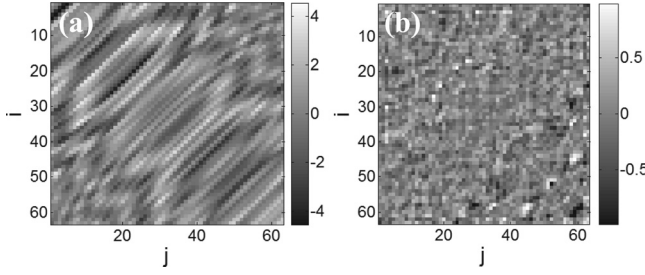


FIG. 5. Separation of single- and multiple-scattering contributions at time  $T = 114 \mu\text{s}$  and frequency  $f = 3.05 \text{ MHz}$ . (a) Real part of  $\mathbf{K}^S$ . (b) Real part of  $\mathbf{K}^M$ .

since single scattering is predominant. As to  $\mathbf{K}^M$ , it displays a random feature as expected for the multiple-scattering contribution [Fig. 5(b)]. However, one cannot conclude that it originates in multiple-scattered waves: It could also correspond to experimental noise.

In order to establish the multiple-scattering origin of  $\mathbf{K}^M$ , we calculated the mean backscattered intensity  $I^M$  as a function of the source–receiver distance  $X = x_j - x_i = m\delta x$  and the arrival time  $T$ ,

$$I^M(X, T) = \left\langle \left| \bar{k}_{ij}^M(T, f) \right|^2 \right\rangle_{f, \{(i,j) | m=j-i\}} \quad (17)$$

The symbol  $\langle \cdot \rangle$  denotes an average over the quantities in the subscript. Here frequency and all source/receiver couples  $(i, j)$  are separated by the same distance  $X$ . In Fig. 6, the spatial dependence of  $I^M$  is compared with the total intensity, at a given time  $T$ . Whereas the total intensity  $I$  shows no preferred direction,  $I^M(X)$  exhibits a typical signature of multiple scattering: The coherent backscattering peak clearly arises around  $X = 0$ . This phenomenon has been widely observed and studied in wave physics (optics,<sup>16,20–26</sup> acoustics,<sup>27–31</sup> and seismology<sup>32–34</sup>). It manifests itself as an enhancement, by a factor 2, in the backscattered intensity at the vicinity of the source (i.e.,  $X = 0$ ). Its physical origin lies in the constructive wave interference between reciprocal paths that have been scattered at least twice; it can only appear when

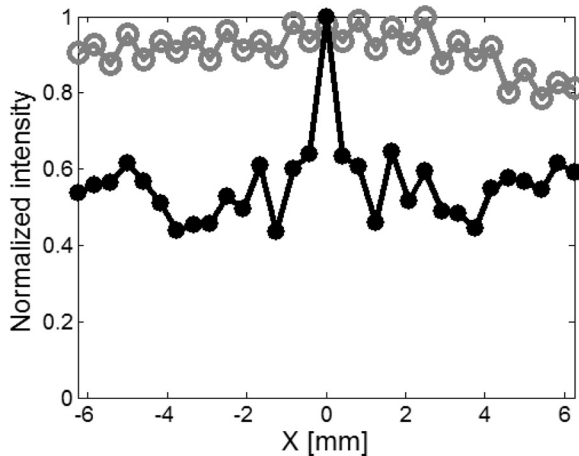


FIG. 6. The multiple-scattering intensity  $I^M$  (black dots) and the total intensity  $I$  (gray circles) are plotted versus  $X$ , at time  $T = 137 \mu\text{s}$ . The intensity profiles have been renormalized with their maximum.

multiple scattering occurs and the reciprocity symmetry is preserved. The intensity profile shown in Fig. 6 is a spectacular evidence of multiple scattering and shows the efficiency of our technique for extracting the multiple-scattering waves among a predominant single-scattering contribution.

Interestingly, though it is weak, the multiple-scattering contribution can be taken advantage of in order to characterize the medium and determine separately the scattering losses and the absorption losses. When a wave propagates through a random medium, it loses progressively its coherence: After traveling over a distance  $L$ , only a fraction,  $\exp(-L/l_{\text{ext}})$ , of the initial energy still propagates in coherence with the initial wave. The parameter  $l_{\text{ext}}$ , called the extinction mean-free path, characterizes the extinction length of the coherent part of the wave. It comes from two distinct phenomena (scattering and intrinsic absorption of the medium) which are associated to two characteristic lengths: The elastic mean-free path  $l_e$  and the absorption mean-free path  $l_a$ , such that

$$\exp(-L/l_{\text{ext}}) = \exp(-L/l_e) \exp(-L/l_a). \quad (18)$$

Experimentally,  $l_{\text{ext}}$  can be determined by measurements of the ensemble-averaged field transmitted through a scattering layer.<sup>35–39</sup> However, this kind of experiment does not allow to distinguish  $l_a$  from  $l_e$ .

We focus on the single- and multiple-scattering intensities obtained at the source:  $I^S(0, T)$  and  $I^M(0, T)$ . They are plotted in Fig. 7. Note that the intensity of the multiple-scattering contribution is less than 1% of the single-scattering contribution. Once  $I^S(0, T)$  and  $I^M(0, T)$  have been measured, we can fit both experimental curves with  $l_a$  and  $l_e$  as independent adjustable parameters. To that end, we need a theoretical model describing the spatial and temporal evolution of the mean intensity inside the random medium. In the literature, the mean intensity is often assumed to obey the diffusion equation.<sup>40</sup> The diffusion approximation is simple but only valid in the long-time limit. Since we deal with a weakly scattering medium, the elastic mean-free path is expected to be very large compared to the scattering path lengths ( $l_e \gg cT$ ). Thus, the diffusion approximation does not apply to our problem. Instead, we used the radiative transfer equation (RTE).<sup>9</sup> Paasschens<sup>41</sup> proposed an exact solution of the RTE in time-domain and real space for an infinite two-dimensional (2D) random medium. Based on this theoretical work, we have computed the exact expression of the single- and double-scattering intensities,  $I^S(0, T)$  and  $I^{(2)}(0, T)$ , as well as an approximate expression of the multiple-scattering intensity  $I^M(0, T)$ , considering the medium as semi-infinite and 2D.<sup>18</sup>

The choice of a 2D model is justified as follows. Experimentally, the transducers are 10 mm in height, which is much larger than the average wavelength (0.5 mm). Moreover, a vertical cylindrical acoustic lens ensures that the emitted beam remains collimated in the  $(x, z)$  plane. Similarly, in reception, only waves propagating in the  $(x, z)$  plane are recorded by the transducers. Thus the single-scattering problem is clearly 2D. As to multiple scattering, for the same reason the only paths that can generate a signal on the receiving transducers are those for which the first and last scatterer

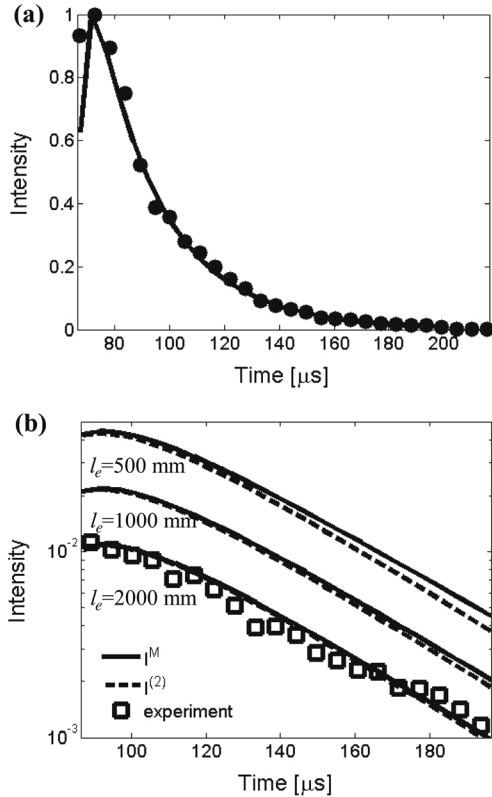


FIG. 7. (a) Single-scattered intensity  $I^S(X = 0, T)$  versus time. Experimental measurements (black circles) are fitted with the theoretical curve (continuous black line) considering an extinction length  $l_{\text{ext}} = 50$  mm. (b) Multiple-scattered intensity  $I^M(X = 0, T)$  versus time. Experimental measurements (white squares) are compared with theoretical results for  $I^M(X = 0, T)$  (continuous black lines) and  $I^{(2)}(X = 0, T)$  (dashed black lines) for different values of the mean-free path, while keeping  $l_{\text{ext}} = 50$  mm. All intensities have been normalized by the maximum of the single-scattered intensity  $I^S(X = 0, T)$  over time.

are in the  $(x, z)$  plane. The gel sample being weakly scattering,  $I^M$  is mostly dominated by double scattering [see Fig. 7(b)]. Thus even though the wave propagation in the gel sample is three-dimensional (3D), we have used the 2D solution for the RTE.

The single-scattering intensity  $I^S(0, T)$  exhibits a temporal evolution which only depends on the extinction length  $l_{\text{ext}}$ .<sup>18</sup> In the case of the gel studied here, the best fit of the experimental results yields  $l_{\text{ext}} = 50$  mm [Fig. 7(a)]. Once  $l_{\text{ext}}$  is known,  $l_e$  and  $l_a$  can be determined by fitting  $I^M(0, T)$  with theory [Fig. 7(b)] with only one adjustable parameter since  $1/l_{\text{ext}} = 1/l_e + 1/l_a$ . The scattering gel is found to be much more absorbing than scattering:  $l_e \sim 2000$  mm, while  $l_a \sim 50$  mm. Figure 7(b) also displays the theoretical evolution of the double-scattering contribution  $I^{(2)}(0, T)$ . For  $l_e \sim 2000$  mm,  $I^{(2)}$  and  $I^M$  are nearly identical, which shows that the double-scattering contribution clearly dominates the multiple-scattering intensity in the gel sample. As the theoretical expression of  $I^{(2)}$  is exact, the measured values of  $l_e$  and  $l_a$  are reliable.<sup>18</sup>

In this example, the medium was a weakly scattering gel, with the ratio  $I^M/I^S$  less than 1%. Yet the separation of single- and multiple-scattering contributions can also be achieved in real scattering media for which  $I^M/I^S$  is closer to unity, as we present in Sec. VI.

## VI. APPLICATION TO HUMAN SOFT TISSUES

The same kind of experiment has been performed in a biological medium for which ultrasound is often used: The breast. The experimental setup is depicted in Fig. 8(a). We use an  $N$ -element ultrasonic array ( $N = 125$ ) with a 4.3-MHz central frequency and a 3.5–5 MHz bandwidth; the array pitch  $\delta x$  is 0.33 mm. The emitted signal is a 0.7- $\mu\text{s}$  sinusoidal burst at  $f_c = 4.3$  MHz. The sampling frequency is 50 MHz. The experimental procedure is the same as in Sec. II. The separation of single- and multiple-scattering contributions can be performed as in Sec. IV, but an adjustment has to be made. Indeed, in our experimental configuration, the array of transducers is placed in the *near-field* of the scattering medium ( $a = 0$ ). Consequently, the entries of matrix  $\mathbf{K}$  are not identically distributed: The variance (i.e., the mean intensity  $I$ ) of  $k_{ij}$  decreases significantly with the distance  $X = x_j - x_i$  between the source and the receiver, as shown by Fig. 9. This implies a different variance for each line of matrix  $\mathbf{A}$ , hence modifying its theoretical distribution of

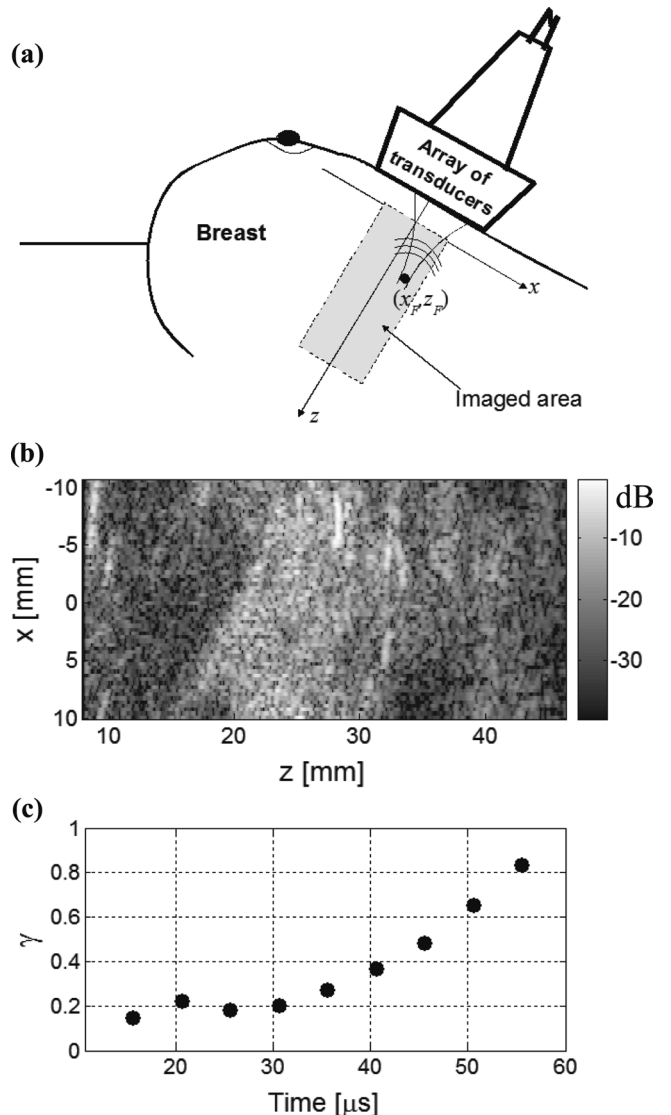


FIG. 8. (a) Experimental setup used for the investigation of multiple scattering in breast tissues. (b) Echographic image of the breast. The gray scale is in decibels. (c) Multiple-scattering rate  $\gamma$  as a function of time.

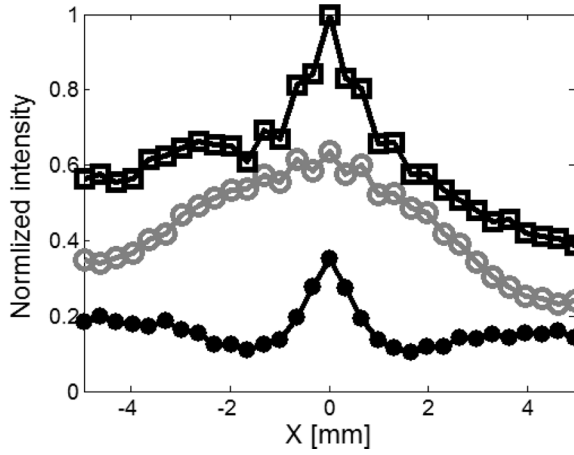


FIG. 9. The multiple-scattering intensity  $I^M(X)$  (black dots), the single-scattering intensity  $I^S(X)$  (gray circles), and the total intensity  $I(X)$  (black squares) are plotted versus  $X$ , at time  $T = 35.6 \mu\text{s}$ . The intensity profiles have been renormalized with the maximum of the total intensity.

singular values. The upper bound  $\lambda_{\max}^{(0)}$  can be computed numerically taking into account this non-uniform distribution of matrix elements.<sup>18</sup> However, this is only possible at the first iteration ( $q = 1$ ). Indeed, whereas the variance of  $\mathbf{A}$  can be estimated, the variance distribution of the subspaces of  $\mathbf{A}$  is unknown *a priori*. Unless we do the (strong) approximation that this variance is uniform, in which case Eq. (13) could be applied, we cannot follow the procedure described in Sec. IV. Here, since  $\mathbf{A}$  clearly has a non-uniform variance, by precaution we choose a different strategy: The same upper bound  $\lambda_{\max}^{(0)}$  is considered at each iteration  $q$  of the single- or multiple-scattering separation process (see Sec. IV). Since  $\lambda_{\max}^{(q)} < \lambda_{\max}^{(0)}$ , this precaution tends to overestimate the threshold and decrease the probability of error.

Figure 9 compares the multiple-scattering, single-scattering, and total intensity profiles, at a given time  $T$ . Contrary to the previous experiment in the gel sample (see Fig. 6), the spatial intensity profiles,  $I(X)$  and  $I^S(X)$ , are not flat due to the *near-field* configuration of the experiment. Once again,  $I^M(X)$  exhibits a coherent backscattering peak on top of a flat incoherent intensity with an enhancement factor close to 2. Interestingly, this indicates that  $\mathbf{K}^M$  is not a noise contribution but does originate from multiple wave scattering in the breast tissue, even though we operate at a frequency (4.3 MHz) for which human soft tissues are usually treated as single scattering.

An ultrasound image of the breast has also been obtained with the same array, using 63-element subapertures [Fig. 8(b)]. As usual in ultrasound imaging, focusing in emission and reception is achieved by applying a set of 63 time delays to the signals transmitted/received by the array. The time delays are computed in order to focus at the desired region of interest, centered at coordinates  $z_F$  and  $x_F$ , assuming that the velocity of sound in soft tissues is known. In the case of breast, as for most soft biological tissues, it is close to that of water ( $c = 1500 \text{ m/s}$ ). Here, 2666 focal planes ( $z_F = 8\text{--}48 \text{ mm}$ ) and 63 values of  $x(x_F = -31\delta x$  to  $x_F = 31\delta x$  with  $\delta x$  the array pitch) have been used. At each depth  $z_F$ , a new set of time delays is calculated; this is more demanding than classical

ultrasound imaging techniques, which generally use the same set of time delays as long as  $z_F$  is within the depth of field. A line of the resulting image represents, in gray level, the amplitude of the total echographic signal at the focal time  $T = 2z_F/c$ , once focused beamforming has been applied to the 63 received signals. The resulting image displays the reflectivity of the medium under investigation. Ultrasound images of human tissues usually reveal the interfaces of inner organs and often exhibit a speckled appearance due to random scattering by subwavelength inhomogeneities (cells, fibers, tissues, etc.).<sup>42</sup> Here the scanned area is particularly echogenic between 30 and 40  $\mu\text{s}$ , corresponding to the depth range from 22.5 to 30 mm. The typical ultrasound image of a human organ (here, the breast) is representative of the amplitude of backscatter at a given time which hopefully (under the single-scattering assumption) corresponds to a given depth, but it does not allow us to distinguish single- and multiple-scattering contributions.

However, once the matrix  $\mathbf{K}$  has been recorded, not only can we build an echographic image, but we can also isolate the multiple-scattering contribution and estimate the multiple-scattering rate  $\gamma$  [Eq. (16)].  $\gamma$  has been averaged over the whole frequency spectrum and is displayed in Fig. 8(c) as a function of time. Figure 8(c) complements the information brought by the echographic image. A relevant observation is that multiple scattering becomes predominant from  $T = 46 \mu\text{s}$ , i.e., to say beyond a depth of 34.5 mm. It means that the single-scattering assumption, upon which the imaging process is based, is incorrect. It does not mean however that the image is totally wrong; a rate  $\gamma$  of 50% means that half of the intensity received by one individual array element comes from multiple scattering. In classical array imaging, each line of the picture is constructed by focused beamforming in emission and reception. This procedure reduces the importance of multiple scattering in the final image because the single-scattered contributions coming from a target in the focal zone add up coherently whereas the contributions from multiple scattering can be expected to be uncorrelated. With  $\gamma = 0.5$  and assuming  $N' = 63$  uncorrelated array elements, the multiple-scattering rate becomes  $\sqrt{\gamma/(1-\gamma)}/N' \sim 1/63$  after beamforming. This is probably an underestimation since multiple-scattering signals cannot be fully uncorrelated.<sup>12,15</sup> As a result, the proportion of multiple scattering in the final image around  $T = 50 \mu\text{s}$  is of the order of a few percents, which is still weak. Also note that at larger times, the technique we presented here would fail: After  $T = 50 \mu\text{s}$ , the rate of multiple scattering becomes too large for the SVD to extract the single-scattering contribution ( $p = 0$ ), at least for some frequencies of the spectrum. As the results are averaged over the whole frequency spectrum (3.5–5 MHz), the multiple-scattering rates that are presented here are still meaningful, until  $T = 60 \mu\text{s}$ . Beyond that time, the method we presented here would be inadequate to separate single and multiple scattering.

## VII. CONCLUSION

The approach we developed here can separate single- and multiple-scattered waves in randomly heterogeneous media. It requires an array of transmitters/receivers and takes

advantage of the persistence of a deterministic coherence of single-scattering signals along the antidiagonals of the interelement matrix. Once a SVD is applied, the single-scattering contribution (signal subspace) is separated from the multiple-scattering contribution (noise subspace) by using a criterion based on RMT. Unlike previous works,<sup>8,12</sup> this technique is particularly well suited for weakly scattering media, for which single scattering dominates. In such media, the technique we presented here is not intended to enhance the quality of the ultrasound image but rather to complement it in two ways. First, the experimental results indicate that this approach can be applied for characterization purposes: The separation of single and multiple scattering provides a way to measure the scattering and absorption mean-free paths independently. This idea was tested on a synthetic gel. Second, the technique was also applied *in vivo* to the case of breast imaging with ultrasonic waves around 4.3 MHz. The occurrence of multiple scattering has been established, and its contribution to the backscattered wave-field is shown to be far from negligible. By measuring the relative amount of multiple scattering, the method serves as an experimental test for the first Born approximation (single scattering), which is usually made in such tissues.

## ACKNOWLEDGMENTS

The authors would like to thank Professor Mickael Tanter for fruitful discussions and Patricia Daenens for her technical help, as well as the *groupe de recherches* Imagerie, Communication et Désordre (IMCODE) of Centre National de la Recherche Scientifique (CNRS, GDR 2253).

<sup>1</sup>B. Angelsen, *Ultrasound Imaging—Waves, Signals and Signal Processing* (Emantec, Trondheim, Norway, 2000), 1416 p.  
<sup>2</sup>S. Stergiopoulos, *Advanced Signal Processing Handbook: Theory and Implementation for Radar, Sonar, and Medical Imaging Real-Time Systems* (CRC Press LLC, Boca Raton, 2001), Sec. 2.  
<sup>3</sup>J. Schmitt, “Optical coherence tomography (OCT): A review,” *IEEE J. Sel. Top. Quantum Electron.* **5**, 1205–1215 (1999).  
<sup>4</sup>S. H. P. Bly, F. S. Foster, M. S. Patterson, D. R. Foster, and J. W. Hunt, “Artifactual echoes in b-mode images due to multiple scattering,” *Ultrasound Med. Biol.* **11**, 99–111 (1985).  
<sup>5</sup>J.-M. Bordier, M. Fink, A. le Brun, and F. Cohen-Tenoudji, “The influence of multiple scattering in incoherent ultrasonic inspection of coarse grain stainless steel,” in *Proceedings of the 1991 Ultrasonics Symposium* (1991), Vol. 2, pp. 803–808.  
<sup>6</sup>B. Karamata, M. Laubscher, M. Leutenegger, S. Bourquin, T. Lasser, and P. Lambelet, “Multiple scattering in optical coherence tomography. I. Investigation and modeling,” *J. Opt. Soc. Am. A* **22**, 1369–1379 (2005).  
<sup>7</sup>B. Karamata, M. Leutenegger, M. Laubscher, S. Bourquin, T. Lasser, and P. Lambelet, “Multiple scattering in optical coherence tomography. II. Experimental and theoretical investigation of cross talk in wide-field optical coherence tomography,” *J. Opt. Soc. Am. A* **22**, 1380–1388 (2005).  
<sup>8</sup>A. Aubry and A. Derode, “Detection and imaging in a random medium: A matrix method to overcome multiple scattering and aberration,” *J. Appl. Phys.* **106**, 044903 (2009).  
<sup>9</sup>M. van Rossum and T. M. Nieuwenhuizen, “Multiple scattering of classical waves: Microscopy, mesoscopy, and diffusion,” *Rev. Mod. Phys.* **71**, 313–371 (1999).  
<sup>10</sup>S. Rytov, Y. A. Kravtsov, and V. Tatarskii, *Principle of Statistical Radiophysics III: Elements of Random Fields* (Springer-Verlag, Berlin, 1989), 249 p.  
<sup>11</sup>S. Rytov, Y. A. Kravtsov, and V. Tatarskii, *Principle of Statistical Radiophysics IV: Wave Propagation Through Random Media* (Springer-Verlag, Berlin, 1989), 198 p.

<sup>12</sup>A. Aubry and A. Derode, “Random matrix theory applied to acoustic backscattering and imaging in complex media,” *Phys. Rev. Lett.* **102**, 084301 (2009).  
<sup>13</sup>A. Tulino and S. Verdù, “Random matrix theory and wireless communications,” *Found. Trends Commun. Inf. Theory* **1**, 1–182 (2004).  
<sup>14</sup>A. M. Sengupta and P. P. Mitra, “Distribution of singular values for some random matrices,” *Phys. Rev. E* **60**, 3389–3392 (1999).  
<sup>15</sup>A. Aubry and A. Derode, “Singular value distribution of the propagation matrix in random scattering media,” *Waves Random Complex Media* **20**, 333–363 (2010).  
<sup>16</sup>D. S. Wiersma, M. P. van Albada, B. A. van Tiggelen, and A. Lagendijk, “Experimental evidence for recurrent multiple scattering events of light in disordered media,” *Phys. Rev. Lett.* **74**, 4193–4196 (1995).  
<sup>17</sup>I. Johnston, “On the distribution of the largest eigenvalue in principal components analysis,” *Ann. Statist.* **29**, 295–327 (2001).  
<sup>18</sup>A. Aubry and A. Derode, arXiv:1003.1963.  
<sup>19</sup>A. Aubry, A. Derode, P. Roux, and A. Tourin, “Coherent backscattering and far-field beamforming in acoustics,” *J. Acoust. Soc. Am.* **121**, 70–77 (2007).  
<sup>20</sup>Y. Kuga and A. Ishimaru, “Retroreflectance from a dense distribution of spherical particles,” *J. Opt. Soc. Am. A* **1**, 831 (1984).  
<sup>21</sup>P.-E. Wolf and G. Maret, “Weak localization and coherent backscattering of photons in disordered media,” *Phys. Rev. Lett.* **55**, 2696–2699 (1985).  
<sup>22</sup>M. P. van Albada and A. Lagendijk, “Observation of weak localization of light in a random medium,” *Phys. Rev. Lett.* **55**, 2692–2695 (1985).  
<sup>23</sup>E. Akkermans, P.-E. Wolf, and R. Maynard, “Coherent backscattering of light by disordered media: Analysis of the peak line shape,” *Phys. Rev. Lett.* **56**, 1471–1474 (1986).  
<sup>24</sup>E. Akkermans, P.-E. Wolf, R. Maynard, and G. Maret, “Theoretical study of the coherent backscattering of light by disordered media,” *J. Phys. France* **49**, 77–98 (1988).  
<sup>25</sup>G. Labeyrie, F. de Tomasi, J.-C. Bernard, C. A. Müller, C. Miniatura, and R. Kaiser, “Coherent backscattering of light by cold atoms,” *Phys. Rev. Lett.* **83**, 5266–5269 (1999).  
<sup>26</sup>G. Labeyrie, C. A. Müller, D. S. Wiersma, C. Miniatura, and R. Kaiser, “Observation of coherent backscattering of light by cold atoms,” *J. Opt. B: Quantum Semiclassical Opt.* **2**, 672–685 (2000).  
<sup>27</sup>G. Bayer and T. Niederdränk, “Weak localization of acoustic waves in strongly scattering media,” *Phys. Rev. Lett.* **70**, 3884–3887 (1993).  
<sup>28</sup>A. Tourin, A. Derode, P. Roux, B. A. van Tiggelen, and M. Fink, “Time-dependent backscattering of acoustic waves,” *Phys. Rev. Lett.* **79**, 3637–3639 (1997).  
<sup>29</sup>K. Sakai, K. Yamamoto, and K. Takagi, “Observation of acoustic coherent backscattering,” *Phys. Rev. B* **56**, 10930–10933 (1997).  
<sup>30</sup>J. de Rosny, A. Tourin, and M. Fink, “Coherent backscattering of an elastic wave in a chaotic cavity,” *Phys. Rev. Lett.* **84**, 1693–1695 (2000).  
<sup>31</sup>J. de Rosny, A. Tourin, A. Derode, P. Roux, and M. Fink, “Weak localization and time reversal of ultrasound in a rotational flow,” *Phys. Rev. Lett.* **95**, 074301 (2005).  
<sup>32</sup>B. A. van Tiggelen, L. Margerin, and M. Campillo, “Coherent backscattering of elastic waves: Specific role of source, polarization, and near field,” *J. Acoust. Soc. Am.* **110**, 1291–1298 (2001).  
<sup>33</sup>L. Margerin, M. Campillo, and B. A. van Tiggelen, “Coherent backscattering of acoustic waves in the near field,” *Geophys. J. Int.* **145**, 593–603 (2001).  
<sup>34</sup>E. Larose, L. Margerin, B. A. van Tiggelen, and M. Campillo, “Weak localization of seismic waves,” *Phys. Rev. Lett.* **93**, 048501 (2004).  
<sup>35</sup>J. H. Page, P. Sheng, H. P. Schriemer, I. Jones, X. Jing, and D. A. Weitz, “Group velocity in strongly scattering media,” *Science* **271**, 634 (1996).  
<sup>36</sup>Z. Q. Zhang, I. P. Jones, H. P. Schriemer, J. H. Page, D. A. Weitz, and P. Sheng, “Wave transport in random media: The ballistic to diffusive transition,” *Phys. Rev. E* **60**, 4843 (1999).  
<sup>37</sup>J. A. Scales and K. van Wijk, “Tunable multiple-scattering system,” *Appl. Phys. Lett.* **79**, 2294–2296 (2001).  
<sup>38</sup>J. A. Scales and A. E. Malcolm, “Laser characterization of ultrasonic wave propagation in random media,” *Phys. Rev. E* **67**, 046618 (2003).  
<sup>39</sup>A. Derode, V. Mamou, and A. Tourin, “Influence of correlations between scatterers on the attenuation of the coherent wave in a random medium,” *Phys. Rev. E* **74**, 036606 (2006).  
<sup>40</sup>E. Akkermans and G. Montambaux, *Mesosopic Physics of Electrons and Photons* (Cambridge University Press, London, 2006), p. 608.  
<sup>41</sup>J. C. J. Paasschens, “Solution of the time-dependent Boltzmann equation,” *Phys. Rev. E* **56**, 1135–1141 (1997).  
<sup>42</sup>C. B. Burckhardt, “Speckle in ultrasound B-mode scans,” *IEEE Trans. Sonics Ultrason.* **25**, 1–6 (1978).